

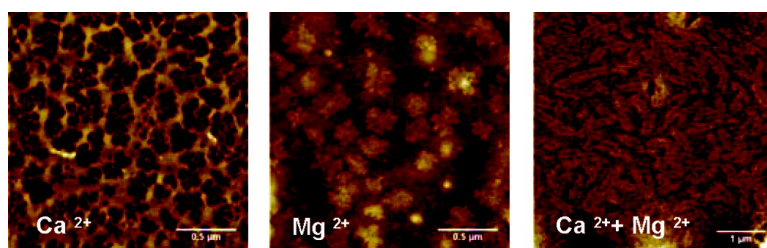
Article

## Divalent Cation-Induced Variations in Polyelectrolyte Conformation and Controlling Calcite Morphologies: Direct Observation of the Phase Transition by Atomic Force Microscopy

Ranjith Krishna Pai, and Saju Pillai

*J. Am. Chem. Soc.*, **2008**, 130 (39), 13074-13078 • DOI: 10.1021/ja803371c • Publication Date (Web): 04 September 2008

Downloaded from <http://pubs.acs.org> on February 8, 2009



### More About This Article

Additional resources and features associated with this article are available within the HTML version:

- Supporting Information
- Access to high resolution figures
- Links to articles and content related to this article
- Copyright permission to reproduce figures and/or text from this article

[View the Full Text HTML](#)

## Divalent Cation-Induced Variations in Polyelectrolyte Conformation and Controlling Calcite Morphologies: Direct Observation of the Phase Transition by Atomic Force Microscopy

Ranjith Krishna Pai<sup>\*,†,‡</sup> and Saju Pillai<sup>†,§</sup>

University of Ulm, Albert-Einstein Allee 11, 89069 Ulm, Germany, Materials Chemistry Research Group, Department of Physical, Inorganic and Structural Chemistry, Arrhenius Laboratory, Stockholm University, SE-106 91 Stockholm, Sweden, and Interdisciplinary Nanoscience Center (iNANO), University of Aarhus, Ny Munkegade, 8000 Aarhus C, Denmark

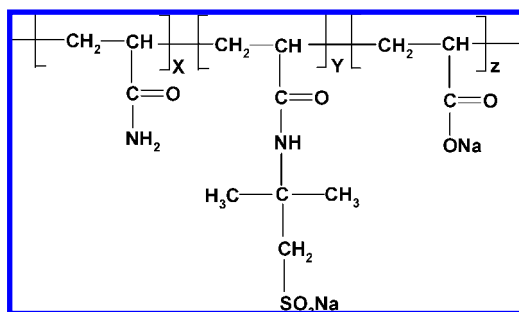
Received May 6, 2008; E-mail: ranjithk@inorg.su.se

**Abstract:** In the biomineralization process, the changes in conformation of organic matrix may be a widespread phenomenon. Investigation of the structural relationship between organic and inorganic materials is the main subject. The approach taken was to extract quantitative information of the variations in polyelectrolyte conformation during the mineralization process using atomic force microscopy. The results infer the evidence of the role of polyelectrolyte conformation in mineralization of calcium carbonate and the methods for understanding the principle that govern biomineralization.

### Introduction

Calcium carbonate ( $\text{CaCO}_3$ ) deposition in biological systems occurs during the formation of mollusc shells,<sup>1</sup> egg shells,<sup>2–4</sup> exoskeletons of arthropods,<sup>5</sup> pearls,<sup>6</sup> and corals.<sup>7</sup> In all these mineralized tissues the organic matrix plays an important role in controlling the orientation, polymorphism, composition, and morphology of the mineral phase. Many studies that were carried out on the mechanisms involved in biomineralization processes and several new biologically inspired synthetic routes were designed to control the formation of the mineral phase.<sup>8,9</sup> It has been shown that polymorphism, morphology, and structural properties of  $\text{CaCO}_3$  can be controlled by the use of specific additives,<sup>10</sup> macromolecules,<sup>11</sup> small organic molecules,<sup>12</sup> and

**Scheme 1.** Chemical Structure of Synthetic Water-Soluble Polyelectrolyte



inorganic ions.<sup>13</sup> Among the inorganic components, magnesium ( $\text{Mg}^{2+}$ ) has a particularly important role in  $\text{CaCO}_3$  precipitation.<sup>14</sup> Biological systems have evolved strategies for high  $\text{Mg}^{2+}$  incorporation and stabilization that yield favorable material properties. In sea urchin spines, for example, the inhomogeneous distribution of  $\text{Mg}^{2+}$  impedes crack propagation, thus enhancing fracture resistance.<sup>15</sup> Under certain thermodynamic conditions,  $\text{Mg}^{2+}$  can act either as an effective inhibitor to nucleation and/or crystal growth of calcite or as a promoter for aragonite nucleation.<sup>16</sup> The inhibition of calcite formation could be explained by the possible preferential adsorption of strongly hydrated  $\text{Mg}^{2+}$  ions onto the growing calcite surfaces or by enhancement of calcite solubility caused by incorporation of  $\text{Mg}^{2+}$  into calcite structure.<sup>17</sup> The role of  $\text{Mg}^{2+}$  as a promoter of aragonite formation is closely related to its ability to inhibit

<sup>†</sup> University of Ulm.

<sup>‡</sup> Stockholm University (Present address).

<sup>§</sup> University of Aarhus (Present address).

- (1) Belcher, A. M.; Wu, X. H.; Christensen, R. J.; Hansma, P. K.; Stucky, G. D.; Morse, D. E. *J. Am. Chem. Soc.* **1996**, *381*, 56–58.
- (2) Fernandez, M. S.; Passalacqua, K.; Arias, J. I.; Arias, J. L. *J. Struct. Biol.* **2004**, *148*, 1–10.
- (3) Lakshminarayanan, R.; Chi-Jin, E. O.; Loh, X. J.; Kini, R. M.; Valiyaveetil, S. *Biomacromolecules* **2005**, *6*, 1429–1437.
- (4) Arias, J. L.; Arias, J. I.; Fernandez, M. S. *Handbook of Biomineralization*; Behrens P., Bäuerlein, E. Eds.; Wiley-VCH Verlag GmbH & Co. KGaA: Weinheim, Germany, 2007; Vol. 2, pp. 109–118.
- (5) Manoli, F.; Koutsopoulos, S. *Dalac, E.* **1997**, *182*, 116–124.
- (6) Xu, G. F.; Yao, N.; Aksay, I. A.; Groves, J. T. *J. Am. Chem. Soc.* **1998**, *120*, 11977–11985.
- (7) Sivakumar, M.; Sampath Kumar, T. S.; Shantha, K. L.; Panduranga Rao, K. *Biomaterials* **1996**, *17*, 1709–1714.
- (8) Lakshminarayanan, R.; Vivekanandan, S.; Samy, R. P.; Banerjee, Y.; Chi-Jin, E. O.; Teo, K. W.; Jois, S. D. S.; Kini, R. M.; Valiyaveetil, S. *J. Am. Chem. Soc.* **2008**, *130*, 4660–4668.
- (9) Pai, R. K.; Pillai, S. *CrystEngComm* **2008**, *10*, 865–872.
- (10) Pai, R. K.; Pillai, S. *Cryst. Growth Des.* **2007**, *7*, 215–217.
- (11) Pai, R. K.; Hild, S.; Ziegler, A.; Marti, O. *Langmuir* **2004**, *20*, 3123–3128.
- (12) Falini, G.; Fermani, S.; Gazzano, M.; Ripamonti, A. *Chem.—Eur. J.* **1977**, *3*, 1807–1814.

- (13) Tong, H.; Ma, W.; Wang, L.; Wan, P.; Hu, J.; Cao, L. *Biomaterials* **2004**, *25*, 3923–3929.
- (14) Sato, K.; Kumagai, Y.; Kogure, T.; Watari, K.; Tanaka, J. *J. Ceram. Soc. Jpn.* **2006**, *114*, 754–759.
- (15) Magdams, U.; Gies, H. *Eur. J. Miner.* **2004**, *16*, 261–268.
- (16) Reddy, M. M.; Wang, K. K. *J. Cryst. Growth* **1980**, *50*, 470–480.

calcite nucleation. When the conditions are such that the formation of calcite nuclei is significantly reduced, the nucleation of the less stable polymorph, aragonite, can take place.<sup>18</sup> Improved understanding of the role of  $Mg^{2+}$  and its incorporation into the calcite lattice has thus attracted considerable interest among materials scientists. Crystallization of  $CaCO_3$  in the presence of  $Mg^{2+}$  in combination with various synthetic polymers has also been investigated as a model of biomineralization.<sup>19–21</sup>

Herein, we report the nucleation of  $CaCO_3$  in the presence or absence of  $Mg^{2+}$  ions in combination with or without synthetic water-soluble poly (acrylamide-*co*-2-acrylamido-2-methyl-1-propane sodium sulfonate-*co*-sodium acrylate) [poly (AM-NaAMPS-SA)] to understand the conformation changes of polyelectrolyte during the mineralization process. Although such investigation have been carried out before by other groups,<sup>22</sup> its mechanisms are still far from being fully understood. This is because the adsorption of organic molecules on a solid surface is a complicated process consisting of many events, such as conformational changes in organic molecules and the coadsorption of ions. To the best of our knowledge there is no report discussing the conformational changes of polyelectrolyte during the mineralization process observed using atomic force microscopy (AFM) in real-time. In the biomineralization process, the conformation changes of the organic matrix may be a widespread phenomenon. The investigation of the structural relationship between organic and inorganic materials is of main interest. The approach taken was to extract quantitative information on the polyelectrolyte conformational changes during the mineralization process using AFM. The results provide evidence of the role of the polyelectrolyte conformation in the mineralization of  $CaCO_3$  and the methods for understanding the principle that govern biomineralization.

## Experimental Section

**Materials.** Acrylamide monomer (B.D.H., U.K) was recrystallized from chloroform and washed with benzene (B.D.H., reagent grade). Then it was dried under vacuum till it reached a constant weight and was stored over silica gel in desiccators. 2-Acrylamido-2-methyl-1-propane sulfonic acid (AMPS), A.R grade (Aldrich), was used as received. The sodium salt of AMPS (NaAMPS) was prepared by dissolving AMPS in stoichiometric quantity of sodium hydroxide solution. Acrylic acid (Aldrich grade) was used as received. Sodium acrylate (SA) was prepared by dissolving acrylic acid in stoichiometric quantity of sodium hydroxide solution. The polyelectrolyte was synthesized by a solution polymerization technique by previously reported methods.<sup>23,24</sup> The solution structure and properties of acrylamide-based polyelectrolyte were reported previously.<sup>25,26</sup> Scheme 1 displays the structure of the [poly(AM-NaAMPS-SA)] (relative viscosity  $\sim 2$ ) with a monomer composition of 80:10:10 which is used as a crystal modifier in this

study. Magnesium chloride, calcium chloride, and potassium carbonate were purchased from Merck. Water was purified by Millipore. A 0.1 M HCl or 0.1 M NaOH buffer was used to adjust the pH.

**Methods. (a) Crystallization of Calcium Carbonates.** In a typical synthesis, a solution of  $CaCl_2$  (2 M, 2 mL) was added to an aqueous solution of poly (AM-NaAMPS-SA) (100 mL, 2.0 g L<sup>-1</sup>), and the pH of the solution [ $CaCl_2$ /poly (AM-NaAMPS-SA)/H<sub>2</sub>O] was adjusted to 7.5 using HCl or NaOH. A solution of  $K_2CO_3$  (2 M, 2 mL) was then added dropwise into the pH-adjusted solution under vigorous stirring for 1 min, and the solution was kept under static conditions in the refrigerator at  $-20^\circ C$ . To study the role of  $Mg^{2+}$  ions on  $CaCO_3$  precipitation, 100 mM of magnesium chloride was added to the aqueous polyelectrolyte solution. In the control experiment both  $Mg^{2+}$  and polymer were omitted.

**(b) Field Emission Scanning Electron Microscopy (FESEM).** SEM studies on the  $CaCO_3$  crystals were carried out using a Hitachi S-5200 field-emission scanning electron microscope at acceleration voltages of 15 or 20 kV after a rotary coating with 3 nm of platinum at an angle of  $45^\circ$  in a Balzers BAF 300. Since the experimental solutions contain KCl, we performed energy dispersive spectroscopy to analyze the chemical composition of the crystals. The results verified the precipitate is  $CaCO_3$  with only little/no K and Cl present.

**(c) Calcium Ion Measurements.** To estimate the polymer/ $CaCO_3$  ratio, we dissolved an aliquot of sample in 0.1 M KCl adjusted to a PH of 6.0 and measured the  $Ca^{2+}$  concentration using  $Ca^{2+}$  selective minielectrodes (ETH 1001). We use the calibration solutions according to Tsien, R.Y. and Rink, T.J.<sup>28</sup> Since ionic strength in our sample and test solutions were equal,  $Ca^{2+}$  concentration rather than  $Ca^{2+}$  activity was determined. The results show that in all samples the amount of polymer was less than 20%.

**(d) X-ray Diffraction Studies.** Powder X-ray diffraction studies on the crystal powder were carried out using a Siemens D500 X-ray diffractometer with Cu K $\alpha$  radiation at 40 kV and 30 mA.

**(e) Raman Spectroscopy.** Raman spectra were recorded using a CRM 200 confocal Raman spectrometer, WiTec, Ulm, Germany. The exciting source was a SGL-2200 laser operating at 532 nm with a power of about 200 mW. The scattered light was collected at an angle of  $180^\circ$  (back-scattering). Typical spectral resolution was 3  $cm^{-1}$ . To avoid the transformation of less stable polymorphs into calcite the laser beam is scanned in a field of  $200 \times 200 \mu m^2$ . The total exposure time was 20 s. Original spectra are normalized to the calcite peak at 280  $cm^{-1}$ . After subtracting the calcite fraction of the spectra the remaining spectra are normalized either to the aragonite or the ACC peak at 205 or 230  $cm^{-1}$ , respectively.

**(f) Atomic Force Microscopy.** An aqueous solution of polyelectrolyte with or without divalent cation dropped on silica were imaged in air using Digital Instruments DI3100 AFM equipped with a Nanoscope IIIa controller (Veeco Instruments, Santa Barbara, CA) operated in TappingMode. A silicon cantilever with resonance frequency 300–400 kHz and spring constant 42 N/m was used. AFM height images were presented after simple flattening using DI software. The samples were observed by AFM immediately after the deposition and also after sample exposure to highly humid atmosphere. Humidity was controlled by enclosing the samples with pure water in a container for 100% relative humidity (RH). The AFM observation was done in the laboratory condition at the relative humidity of 50–60%. It should be noted that it is hard to attach negatively charged polyelectrolyte on a negatively charged Si surface because of electrostatic repulsive forces. However, under relatively high polyelectrolyte concentration, van der Waals attraction to the adsorbing surface could overwhelm electrostatic repulsive

- (17) Albeck, S.; Aizenberg, J.; Addadi, L.; Weiner, S. *J. Am. Chem. Soc.* **1993**, *115*, 11691–11697.  
 (18) Fernandez Diaz, L.; Putnis, A.; Prieto, M.; Putnis, C. V. *J. Sediment. Res.* **1996**, *66*, 482–491.  
 (19) Meldrum, F. C.; Hyde, S. T. *J. Cryst. Growth* **2001**, *231*, 544–558.  
 (20) Loste, E.; Wilson, R. M.; Seshadri, R.; Meldrum, F. C. *J. Cryst. Growth* **2003**, *254*, 206–218.  
 (21) Falini, G.; Gazzano, M.; Ripamonti, A. *J. Cryst. Growth* **1994**, *137*, 577–584.  
 (22) Choi, C. S.; Kim, Y. W. *Biomaterials* **2000**, *21*, 213–222.  
 (23) Turner, S. R.; Siano, D. B.; Bock, J. U.S. Patent 4,520,182, 1985.  
 (24) Durmaz, S.; Okay, O. *Polymer* **2000**, *41*, 3693–3704.  
 (25) McCormick, C. L.; Johnson, C. B.; Tanaka, T. *Polymer* **1988**, *29*, 731.  
 (26) McCormick, C. L.; Blackmon, K. P. *J. Polym. Sci., Polym. Chem.* **1986**, *24*, 2635.

- (27) Pai, R. K. Synthesis and Characterization of Polymer-Mediated Biomimetic Calcium Carbonate Materials. Ph.D. Dissertation, University of Ulm, Ulm, Germany, 2005.  
 (28) Tsien, R. Y.; Rink, T. J. *J. Biochim. Biophys. Acta* **1980**, *599*, 623–638.

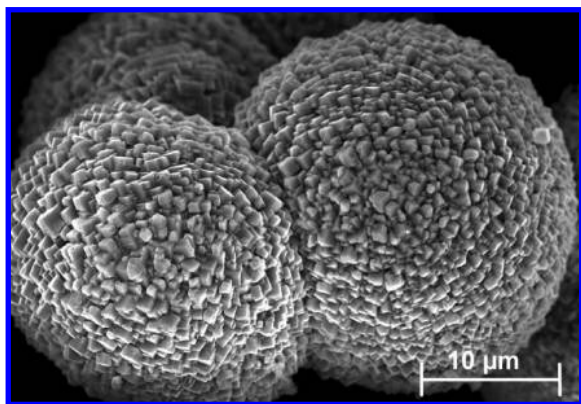


**Figure 1.** Representative SEM images of the CaCO<sub>3</sub> crystal aggregates grown in the presence of polyelectrolyte without magnesium.

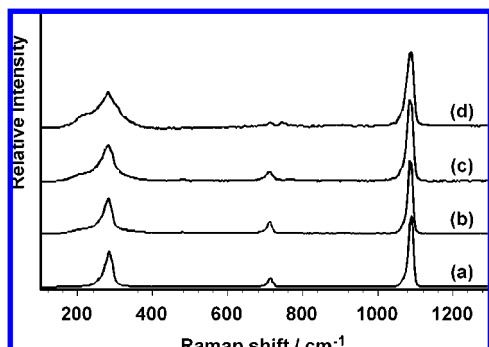


**Figure 2.** Raman spectra (without subtracting the calcite spectra) recorded from (a) CaCO<sub>3</sub> standard and CaCO<sub>3</sub> precipitated in the presence of (b) polyelectrolyte without Mg<sup>2+</sup>, (c) with Mg<sup>2+</sup> without polyelectrolyte, and (d) with polyelectrolyte and Mg<sup>2+</sup>.

forces and force the polymers onto the Si surface, which allow the imaging of polyelectrolyte surface.

## Results and Discussion

CaCO<sub>3</sub> precipitation in the absence of Mg<sup>2+</sup> or polyelectrolyte resulted in the anticipated calcite rhombohedral morphologies. Crystallization in the presence of polyelectrolyte without Mg<sup>2+</sup> resulted in the formation of aggregates of spherical crystal morphology with diameter 20 μm (see Figure 1). These spheres consist of rhombohedra subcrystals with sizes of 1 μm. Raman spectra and XRD (Figures 2b and 3a) show clearly that only the calcite polymorph is present in these spherical aggregates. Here the spherical crystal morphology might result from polyelectrolyte via specific or nonspecific crystal-additive interactions. The influence of Mg<sup>2+</sup> on the growth of CaCO<sub>3</sub> in the absence of polyelectrolyte was more striking. The resulting precipitates had four different morphologies: spindle-like, dumbbell-like (Cölfen, H et al.<sup>29</sup> also obtained similar morphology by using double-hydrophilic block copolymer PEG-b-PMAA as an additive), cross-like, and mulberry like (Grassmann et al.<sup>30</sup> observed similar CaCO<sub>3</sub> morphology grown within gelatin and artificial p-AAm gel matrices in the presence of p-L-Asp). Their sizes were in the range between 3 and 4 μm (Figure 4a A–D). The texture of these crystal aggregates were roughened, and the subcrystals appear as intergrown rhombohedra (with sizes of 200 nm) with well-defined {10.4} faces.

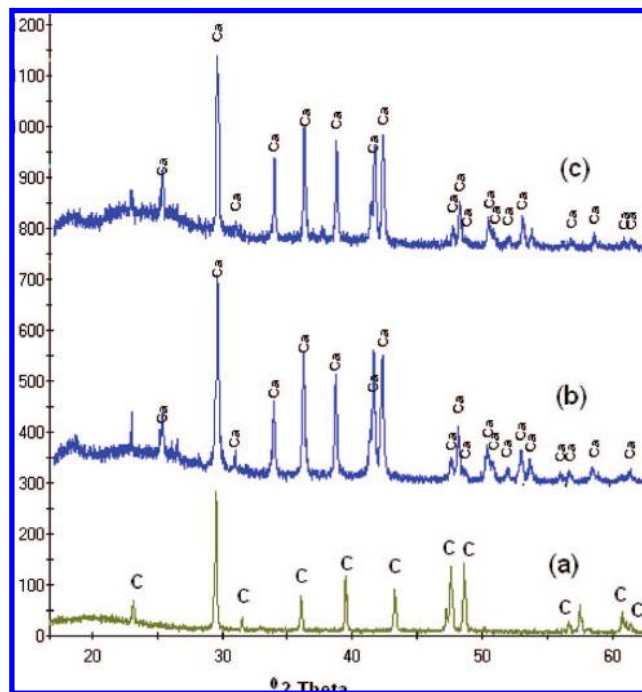


**Figure 3.** XRD spectra recorded from CaCO<sub>3</sub> precipitated in the presence of (a) polyelectrolyte without Mg<sup>2+</sup>, (b) with Mg<sup>2+</sup> without polyelectrolyte, and (c) with polyelectrolyte and Mg<sup>2+</sup>.

The presence of calcite, aragonite, and amorphous calcium carbonate (ACC) was confirmed by Raman analysis; whereas X-ray diffraction (XRD) indicated the presence of calcite only (Figure 2c and Figure 3b, respectively). Raman analysis was particularly valuable for detecting amorphous and hydrated phases of CaCO<sub>3</sub>; XRD was more sensitive for the identification of crystalline phases.<sup>9,20</sup> After subtracting the calcite fraction, aragonite and ACC peaks can clearly be seen in the remaining spectra (Figure 5b,e). Loste et al.<sup>20</sup> have shown that the increase in the Mg<sup>2+</sup> content of the solution results in the precipitation of intergrown rhombohedral crystal aggregates and significant changes in the shape of the aggregates occurred upon increasing the Mg<sup>2+</sup> or by combining organic plus Mg<sup>2+</sup> additives. In contrast, the concentration of Mg<sup>2+</sup> to Ca<sup>2+</sup> ratio was kept constant and then, by combining the polyelectrolyte plus Mg<sup>2+</sup>, resulted in the same morphologies that were found with Mg<sup>2+</sup> alone (Figure 4b, A–D). However the addition of polyelectrolyte induces the smooth texture as well as reduction in crystal aggregate size which were markedly different in texture and size from the crystal aggregates produced with Mg<sup>2+</sup> alone. The crystal aggregate sizes were between 2 and 2.5 μm, and the spherical-shaped subcrystals with diameters in the range of 100 nm appeared on the surface. The XRD pattern recorded shows the presence of only calcite crystals (Figure 3c). Nevertheless, in the Raman spectrum a shoulder appears at 200 cm<sup>-1</sup> (Figure 2d) indicating the presence of aragonite. After subtracting the calcite fraction aragonite, peaks at 209, 705, and 1087 cm<sup>-1</sup> can clearly be seen in the remaining spectrum (Figure 5c). In addition to this several peaks for ACC were observed in Raman analysis after subtracting the calcite fraction (Figure 5f). The formation of calcite and aragonite from transient phases of ACC was demonstrated in echinoderms and mollusks.<sup>31,32</sup> ACC is a

(29) H.Cölfen, Qi, L. *Chem.—Eur. J.* **2001**, *7*, 106.

(30) Grassmann, O.; Müller, G.; Löbmann, P. *Chem. Mater.* **2002**, *14*, 4530–4535.

(31) Beniash, E.; Aizenberg, J.; Addadi, L.; Weiner, S. *Proc. R. Soc. London, Ser. B* **1997**, *264*, 461–465.

(32) Addadi, L.; Raz, S.; Weiner, S. *Adv. Mater.* **2003**, *15*, 959–970.

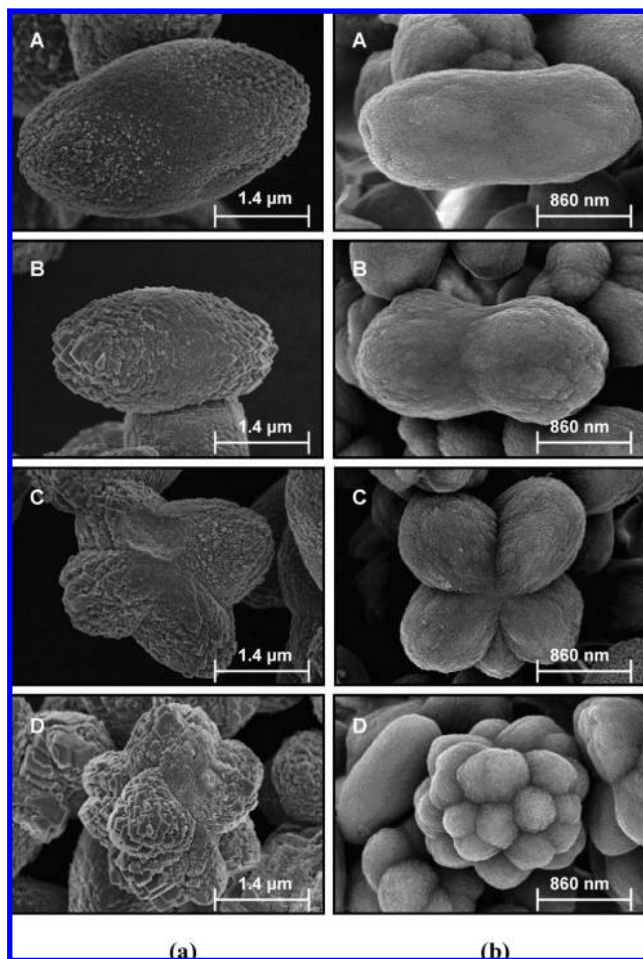


**Figure 4.** Representative SEM images of the  $\text{CaCO}_3$  crystal aggregates grown in the presence of (a, A–D) magnesium without polyelectrolyte and (b, A–D) in combination with magnesium and polyelectrolyte.

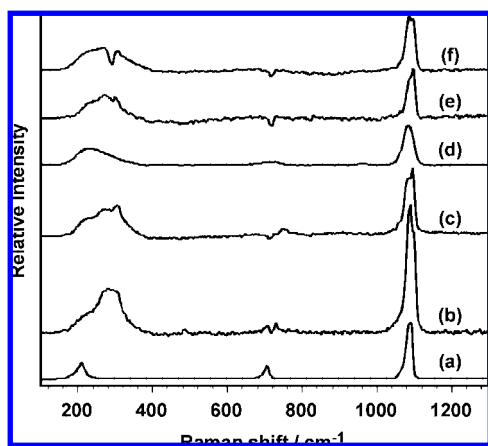


**Figure 5.** After subtracting the calcite spectra, the remaining Raman spectra show (a) aragonite reference and (d) amorphous calcium carbonate (ACC) reference peaks.  $\text{CaCO}_3$  precipitated in the presence of (b)  $\text{Mg}^{2+}$  without polyelectrolyte and (c) polyelectrolyte and  $\text{Mg}^{2+}$  show Aragonite peaks; whereas  $\text{CaCO}_3$  precipitated in presence of (e)  $\text{Mg}^{2+}$  without polyelectrolyte and (f) polyelectrolyte and  $\text{Mg}^{2+}$  show ACC peaks.

metastable phase that normally transforms within minutes into a stable crystalline phase. Our samples from both experiments ( $\text{Mg}^{2+}$  alone and  $\text{Mg}^{2+}$  with polyelectrolyte) consist of a mixture of calcite, aragonite, and ACC, which indicates this transformation process is present. Our explanation for more than one phase

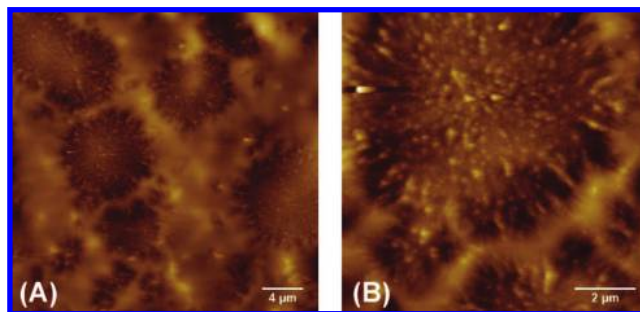


**Figure 6.** AFM images of an aqueous polyelectrolyte surface that shows some phase separation: a lower spherical area and an upper cloudy area. A high charge density on the polymer backbone produces a high electrostatic potential around it, and a fraction of counterions are consequently located in the immediate vicinity of the polyelectrolyte chain leading to phase separation.

that induced by the  $\text{Mg}^{2+}$  alone can be the initial transient ACC phase might contain low concentration of  $\text{Mg}^{2+}$  that is very different from what was expected for the selective nucleation for aragonite. Under these conditions precipitation is rapid since it is barely inhibited by the small  $\text{Mg}^{2+}$  concentration, but the  $\text{Mg}^{2+}$  concentration is sufficient to induce the shape of the aggregates of  $\text{CaCO}_3$ . The mixture of  $\text{CaCO}_3$  phases induced by  $\text{Mg}^{2+}$  alone resembled that induced by the  $\text{Mg}^{2+}$  with polyelectrolyte. However, it is noteworthy that crystals grown in the presence  $\text{Mg}^{2+}$  with polyelectrolyte exhibited much smoother texture or spherical-shaped subcrystals, as well as reduction in crystal aggregates size, than those formed in the  $\text{Mg}^{2+}$  alone. The results obtained in the present work indicate that the crystalline structures and the shape of the  $\text{CaCO}_3$  aggregates are mostly driven by  $\text{Mg}^{2+}$  alone. However the smooth texture as well as reduction in crystal aggregates size could be due to the change in the chemical environment at the polyelectrolyte surface when the aggregates come in contact with  $\text{Mg}^{2+}$ .

AFM has been used to examine the variation of the poly-electrolyte conformation, when they come in contact with divalent cations. We first discuss the AFM imaging on dilute aqueous polyelectrolyte surface, in the absence of divalent cations. Figure 6 shows the typical tapping mode AFM images of a polyelectrolyte surface. Here we could see some phase separation: a lower spherical area and an upper cloudy area. Poly (AM-NaAMPS-SA) possess ionizable groups, which dissociate in aqueous media to give negatively charged poly-electrolyte chains and positively charged counterions. The repulsion between charged monomers tends to expand the polyelectrolyte chain. A high charge density on the polymer backbone produces a high electrostatic potential around it, and a fraction of counterions are consequently located in the immediate vicinity of the polyelectrolyte chain leading to phase separation, if counterions are multivalent.<sup>33–35</sup> It is assumed that the introduction of  $\text{Ca}^{2+}$  to the polyelectrolyte solution will induce the formation of complexes with the sulfonate ( $-\text{SO}_3^{2-}$ ) groups and organize the polyelectrolyte backbone into a spherically orientated state. Conformational changes could affect the channels that facilitate the transport of ions, thus controlling the binding of ions and the active sites on the surface of the

(33) Michaeli, I. *J. Polym. Sci.* **1960**, 291.

(34) Ikegami, A.; Imai, N. *J. Polym. Sci.* **1962**, 56, 133.

(35) Kimizuka, H.; Yamauch, A.; Mori, T. *Bull. Chem. Soc. Jpn.* **1967**, 40, 1281.

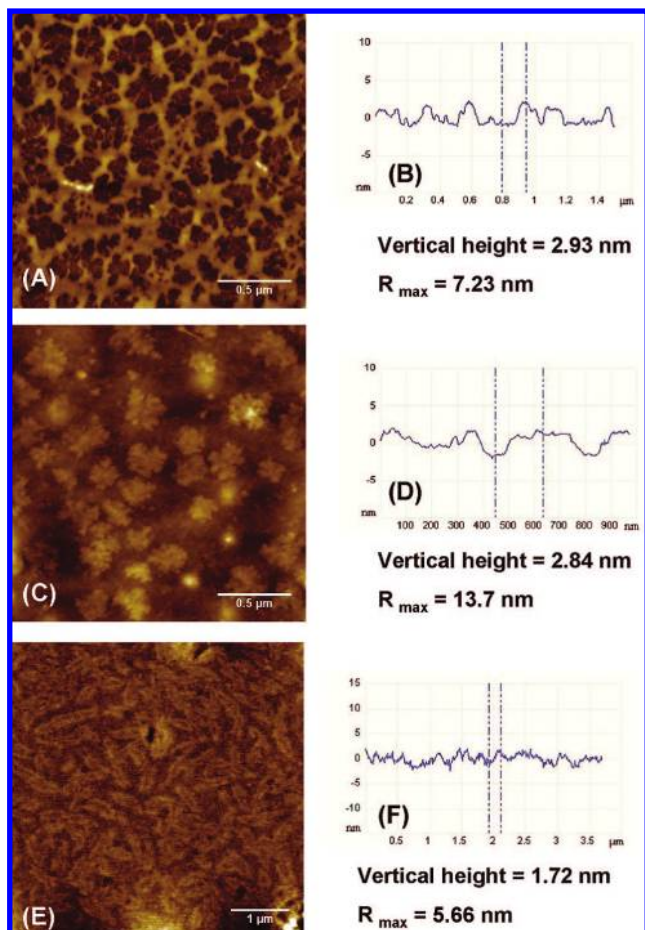


**Figure 7.** AFM images of aqueous polyelectrolyte surface with (A) calcium ions that shows collapsed region and its several branches, (C) magnesium ions that show that the branches only appear as a corona around the core, which assumes a gradually tapering shape toward each end. No single branches can be seen anymore, as is for a collapsed conformation of the polyelectrolyte. (E) Magnesium and calcium ions show  $\text{Ca}^{2+}$  and  $\text{Mg}^{2+}$  ions lead to a more pronounced tapered region, which indicates conformational freedom in the denatured state. Panels B, D, and F are the corresponding vertical height profiles.

polyelectrolyte that could be altered, thus affecting the nucleation pattern. This assumption is supported by AFM results. The influence of calcium ( $\text{Ca}^{2+}$ ) and magnesium ( $\text{Mg}^{2+}$ ) on the polyelectrolyte solution is depicted in Figure 7A,C; a marked conformational change is seen. In particular, a rather small fraction of divalent cations is already sufficient to lead to a collapse of the polyelectrolyte in solution. At sufficiently high salt concentration, the two systems (polyelectrolyte– $\text{Ca}^{2+}$ , polyelectrolyte– $\text{Mg}^{2+}$ ) enter a two-phase region, which yield a polyelectrolyte-rich gel-like precipitate and a virtually polymer-free aqueous phase. The large majority of the cations are expected to be located inside the collapsed regions. In Figure 7A, we could see the adsorbed polyelectrolyte with  $\text{Ca}^{2+}$  ions. The core of the collapsed globular region and its several branches are clearly visible. This orientation may lead to the formation of aggregates of spherical crystal morphology (Figure 1) and points out the fact that the polymer provides nucleating sites for crystal growth through complexation of  $\text{Ca}^{2+}$  by the  $-\text{SO}_3^{2-}$  groups on the backbone, and it also acts as a growth-

directing agent. Figure 7C displays the image of the same polyelectrolyte in the presence of  $\text{Mg}^{2+}$  ions. Now the branches only appear as a corona around the core, which assumes a gradual tapering toward each end. No single branches can be seen anymore, as is for a collapsed conformation of the polyelectrolyte. This type of orientation may lead to the formation of “spindle-like” aggregates with Mg-containing calcite. The crystal morphology change caused by the presence of  $\text{Mg}^{2+}$  can be a slow process. As we can see, the crystal aggregates in Figure 4 panels a,A and b,A have not reached their stable morphology because the faces have not disappeared completely. We can expect that the final morphology of a crystal could be a mulberry-like shape as shown in Figure 4 panels a,D and 4b,D. The growth rates are different at different stages of the morphology change.<sup>36</sup> We believe that once the crystal morphology reaches its equilibrium state, the crystal growth rate will become constant and the amount of  $\text{Mg}^{2+}$  incorporated at this stage will be uniform. Figure 7E demonstrates that, at parallel polyelectrolyte concentration and pH, the addition of both the  $\text{Ca}^{2+}$  and  $\text{Mg}^{2+}$  ions leads to a more pronounced tapered region, which indicates conformational freedom in the denatured state. Such conformational change could be due to the strong interaction of  $\text{Mg}^{2+}$  ions with the polyelectrolyte. The addition of  $\text{Mg}^{2+}$  ions weakened the interaction between the polyelectrolyte and the  $\text{Ca}^{2+}$  ions since  $\text{Mg}^{2+}$  ions possess high charge density. Perhaps because of this, most of the  $\text{Ca}^{2+}$  ions are preferentially confined within the collapsed region. Therefore, we can assume that such an orientation of the side-chain functional groups on the polyelectrolyte backbone plays a crucial role for the selective morphogenesis of the crystal aggregates with smooth texture and reduction in crystal aggregates size.

## Conclusion

Our observations showed that we could describe the alteration of  $\text{CaCO}_3$  crystal aggregates’ shape and texture as well as size by divalent cation with or without a polyelectrolyte having preorganized structure prior to mineral deposition, and their roles in regulating the growth of calcium carbonate minerals. Though the investigation of the structural relationship between organic and inorganic layers is far from complete, such structural and textural changes as well as size changes are roughly consistent with the effect of conformation on the obtained calcite morphology. In conclusion, our results show the particle structure, texture, and size can alter via conformational freedom in the denatured state prior to mineral deposition, and the mode of orientation varies with nature of additives. These results provide a relationship between the effect of conformational changes on the microstructure of  $\text{CaCO}_3$  composites and the necessity of new synthetic strategies. These model experiments serve to demonstrate the complexity of crystal growth in biological systems.

**Acknowledgment.** The work described in this paper was carried out during the framework of R. K. Pai’s doctoral degree program at the University of Ulm, Germany. The work was financially supported by the Graduate College “Molecular Organization and Dynamics at Interfaces”.

JA803371C

(36) Zhang, Y.; Dawer, R. A. *Chem. Geol.* **2000**, *163*, 129–138.